pubs.acs.org/Biomac

Article

# Protein Vesicles with pH-Responsive Disassembly

Dylan R. Dautel, William T. Heller, and Julie A. Champion*

Cite This: https://doi.org/10.1021/acs.biomac.2c00562

Read Online

ACCESS | Metrics & More | Article Recommendations | Supporting Information

**ABSTRACT:** Protein biomaterials offer several advantages over those made from other components because their amino acid sequence can be precisely controlled with genetic engineering to produce a diverse set of material building blocks. In this work, three different elastin-like polypeptide (ELP) sequences were designed to synthesize pH-responsive protein vesicles. ELPs undergo a thermally induced hydrophobic transition that enables self-assembly of different kinds of protein biomaterials. The transition can be tuned by the composition of the guest residue, X, within the ELP pentapeptide repeat unit, VPGXG. When the guest residue is substituted with an ionizable amino acid, such as histidine, the ELP undergoes a pH-dependent hydrophobic phase transition. We used pH-responsive ELPs with different levels of histidine substitution, in combination with leucine zippers and globular, functional proteins, to fabricate protein vesicles. We demonstrate pH-dependent self-assembly, diameter, and disassembly of the vesicles using a combination of turbidimetry, dynamic light scattering, microscopy, and small angle X-ray scattering. As the ELP transition is dependent on the sequence, the vesicle properties also depend on the histidine content in the ELP building blocks. These results demonstrate the tunability of protein vesicles endowed with pH responsiveness, which expands their potential in drug-delivery applications.

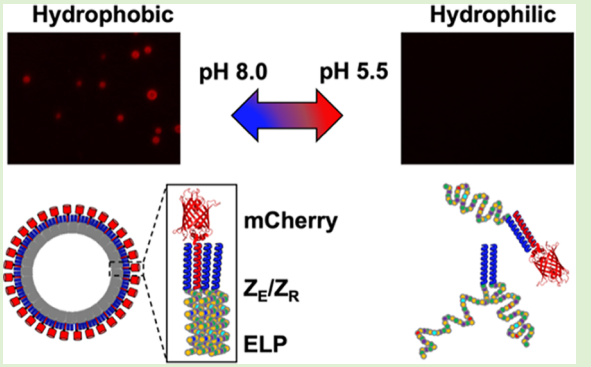




## INTRODUCTION

Lipid and polymeric vesicles have been used as drug-delivery vehicles, microbioreactors, and artificial organelles.[1−4] Lipid vesicles (liposomes) are well studied and have been translated into clinical applications due to their ability to load and deliver cargo and their inherent biocompatibility.[5] However, they have poor stability and limited tunability compared to polymeric vesicles (polymersomes).[6] Vesicles synthesized from many different types of polymers have been well characterized and are generally recognized for their high stability and tunability but lack inherent biological activity. To broaden polymersome use, stimuli-responsive polymers have been used as building blocks, endowing vesicles with new properties. This strategy has been used to design polymersomes that are responsive to changes in pH, ionic strength, light, and temperature.[7−9] These properties make polymersomes useful tools for drug delivery, separations, and microreactor applications, as they can retain their structure for long time periods and then be triggered to disassemble or release cargo under specified conditions. pH-sensitive biomaterials including liposomes, polymersomes, lipoplexes, and others have been designed for pH disassembly, mainly for drug-delivery applications due to acidification of tissues associated with cancer, inflammation, and infection and acidification of endosomes in the intracellular trafficking pathway.[10−13]

Proteins offer both the biocompatibility of lipids and the tunability of polymers, with the advantage of inherent biofunctionality, such as specific binding or enzymatic activity. Elastin-like polypeptides (ELPs) are one kind of protein building block used in the development of a wide range of biomaterials, including nanoparticles, micelles, and vesicles.[14−20] ELPs are tunable proteins that consist of $n$ pentapeptide repeats of the amino acid sequence $(VPGXG)_n$, where the guest residue, X, can be any amino acid except proline.[15] ELPs undergo hydrophobic conformational changes when heated above a characteristic transition temperature ($T_t$), resulting in coacervation of the ELP.[21−23] The $T_t$ is dependent on ELP length $n$, ELP concentration, the concentration and identity of co-solutes, and the composition of the guest residue X.[24−28] The guest residue can be used to tune ELP hydrophobicity, cross-linking capabilities, or pH responsiveness.[26,29,30] The effect of altering the guest residue on $T_t$ has been well documented and has been used to develop a hydropathy index for all 20 amino acids quantified by the $T_t$ of ELPs.[26]

Previous work in our lab has investigated the self-assembly of vesicles solely from two fusion protein constructs, $Z_R$-ELP and globule-$Z_E$.[29,31−34] In this system, the globule represents

Received: May 3, 2022
Revised: July 15, 2022

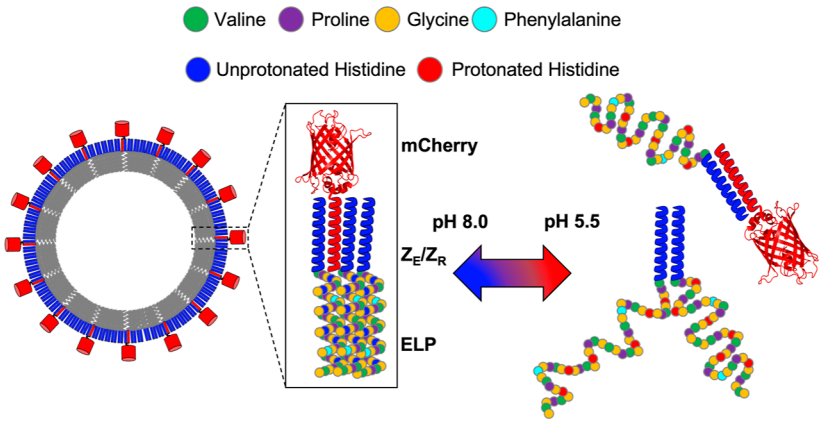


**Figure 1.** Schematic of the proposed vesicle disassembly caused by the protonation of histidine in acidic environments. The ELP shown represents $H_{15}$-$Z_R$-ELP, but only shows 10 of the 25 total pentapeptide repeats for simplicity.

globular, hydrophilic proteins ranging from fluorescent proteins to enzymes that endow vesicles with biofunctionality. The ELP serves as the hydrophobic component of the vesicles and drives vesicle self-assembly through a transient coacervate phase when the protein solution is heated from 4 to 25 °C. The glutamate- and arginine-rich leucine zippers, $Z_E$ and $Z_R$, link the hydrophobic ELP domain to the hydrophilic globular domain with femtomolar affinity,[35] creating amphiphiles that self-assemble into vesicles. The vesicles are composed of a single layer with a hydrophilic shell of globular protein on the exterior and hydrophobic ELP on the interior.[34] Due to the behavior of ELPs, self-assembly of vesicles is dependent on ionic strength, protein concentration, temperature, and composition of the ELP guest residue.[29,34,36] Vesicle self-assembly also depends on the characteristics of the globular protein due to the molecular packing constraints of the amphiphiles including the molar ratio of globule-$Z_E$ to $Z_R$-ELP ($Z_E/Z_R$ ratio).[31,32]

Here, we incorporated the ionizable amino acid histidine into the guest residue of ELP to develop pH-sensitive vesicles. Ionizable amino acids in the guest residues of ELP have been shown to induce pH-dependent reverse hydrophobic phase transition and have been used for disassembly of ELP micelles in vivo.[12,13] Protonation of the imidazole side chain of histidine ($pK_a$ 6.0) begins as the pH decreases from basic to neutral. As the pH decreases further, the fraction of the protonated histidine increases until the imidazole side chains are nearly fully protonated around pH 5.0. When histidine is incorporated into the guest residue of ELP, it allows for pH-dependent phase transition of the ELP due to the increased solubility of the charged ELP at reduced pH.[26,30] Therefore, protein vesicles made from histidine-substituted ELPs should disassemble under acidic conditions due to the protonation state of histidine (Figure 1). To develop a range of pH-responsive vesicles, we designed three ELP variants by altering the guest residue from valine to histidine. The variants, $H_5$-$Z_R$-ELP, $H_{10}$-$Z_R$-ELP, and $H_{15}$-$Z_R$-ELP, have 5, 10, and 15 total histidines in the 25 pentapeptide repeats (Table 1). To determine the effect of pH on each H-$Z_R$-ELP variant, protein solutions containing mCherry-$Z_E$ as the hydrophilic domain and H-$Z_R$-ELP were characterized by turbidity, dynamic light scattering (DLS), epifluorescence microscopy, and small angle X-ray scattering (SAXS). This work demonstrates the tunability of pH-responsive globular protein vesicles and develops protein vesicles capable of disassembly under physiological and disease relevant conditions, with potential for future applications in drug delivery.

**Table 1. Abbreviations of all H-$Z_R$-ELP Variants Used in This Work and Corresponding Amino Acid Sequence**

| ELP name | ELP sequence |
|---|---|
| $Z_R$-ELP | [VPGVG VPGVG VPGFG VPGVG VPGVG]$_5$ |
| $H_5$-$Z_R$-ELP | [VPGVG VPG**H**G VPGFG VPGVG VPGVG]$_5$ |
| $H_{10}$-$Z_R$-ELP | [VPGVG VPG**H**G VPGFG VPG**H**G VPGVG]$_5$ |
| $H_{15}$-$Z_R$-ELP | [VPG**H**G VPG**H**G VPGFG VPG**H**G VPGVG]$_5$ |

## EXPERIMENTAL SECTION/METHODS

**Protein Expression.** The plasmids pQE60/$His_6$-$Z_E$/$H_5$-$Z_R$-ELP, pQE60/$His_6$-$Z_E$/$H_{10}$-$Z_R$-ELP, pQE60/$His_6$-$Z_E$/$H_{15}$-$Z_R$-ELP, and pET28a/$His_6$-sfGFP-$Z_E$ were obtained from Genscript, and pQE60/mCherry-$Z_E$ was obtained through PCR, as described in a previous work.[37] The plasmid pQE60/$His_6$-$Z_E$/$H_5$-$Z_R$-ELP was a kind gift of Profs. D.A. Tirrell and K. Zhang. The plasmids were transformed into heat-competent AF-IQ *Escherichia coli*. The AF-IQ *E. coli* strain is a phenylalanine-auxotrophic strain that has been used to insert a non-canonical amino acid into $Z_R$-ELP, which allowed for photo-cross-linking.[29] In this work, AF-IQ was used out of convenience and no non-canonical amino acid was inserted into any of the H-$Z_R$-ELPs. Cells were grown by inoculating 5 mL of overnight culture in 1 L of lysogeny broth (LB) media containing 200 mg/L ampicillin and 34 mg/L chloramphenicol. The culture was grown at 37 °C until it reached an OD at 600 nm of 0.6 to 0.8. Then, expression was induced by addition of 1.0 mM isopropyl beta-D-1-thiogalactopyranoside (IPTG). After 5 hours of expression, the protein was harvested by centrifugation at 4000*g* for 10 min and pellets were stored at −80 °C.

**Protein Purification.** H-$Z_R$-ELP and $Z_R$-ELP pellets from 1 L of culture were lysed on ice in 80 mL of lysis buffer containing 8 M urea buffered by 50 mM trisCl at pH 8.0 by sonication. Lysate was cleared by centrifugation at 10,000*g* for 30 min then incubated with Ni-NTA beads (Qiagen) for 1 h, while rotating at 4 °C to bind the His-tagged protein. The Ni-NTA beads were then loaded onto an econo-pac column (BioRad) and washed with 8 M urea, pH 6.3, until no protein was present in the wash as measured by absorbance at 280 nm (A280) using a NanoDrop 2000. Protein was eluted by disrupting the leucine zipper interaction with buffer containing 6 M GuHCl, 50 mM trisCl, and 40 mM imidazole at pH 8.0. Yields were approximately 40 mg/L. mCherry-$Z_E$ and sfGFP-$Z_E$ were purified in a similar manner except using native conditions. mCherry-$Z_E$ was lysed in 10 mM imidazole, 300 mM NaCl, and 100 mM $Na_2HPO_4$, washed in 20 mM imidazole, and eluted in 250 mM imidazole. After purification, H-$Z_R$-ELP was dialyzed into mQ water with six buffer changes over 2 days using a SpectraPor 3.5 kDa molecular weight cutoff membrane. Similarly, mCherry-$Z_E$ was buffer exchanged into PBS by dialysis with three buffer


https://doi.org/10.1021/acs.biomac.2c00562
Biomacromolecules XXXX, XXX, XXX−XXX

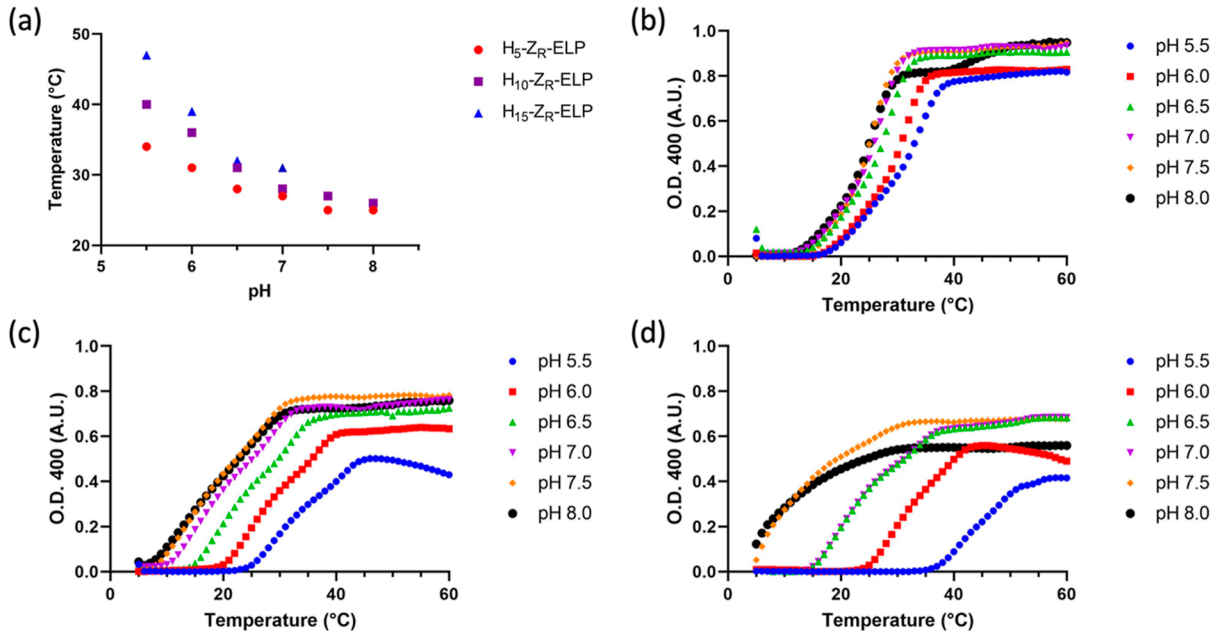


**Figure 2.** Transition temperature of 30 $\mu$M $H_5$-$Z_R$-ELP, $H_{10}$-$Z_R$-ELP, and $H_{15}$-$Z_R$-ELP in aqueous solutions containing 1.5 $\mu$M mCherry-$Z_E$ (0.05 $Z_E$/$Z_R$ ratio), 0.5 M NaCl, and either 10 mM sodium phosphate or sodium succinate depending on the pH of the solution. (a) Transition temperature of each $Z_R$-ELP variant as a function of pH. (b) Representative turbidity vs temperature profiles of $H_5$-$Z_R$-ELP, (c) $H_{10}$-$Z_R$-ELP, and (d) $H_{15}$-$Z_R$-ELP at pH between 5.5 and 8.0.

changes, followed by overnight dialysis using a Spectra/Por 12−14 kDa molecular weight cutoff membrane. The purity of proteins was assessed using sodium dodecylsulfate polyacrylamide gel electrophoresis (Figure S1).

**Transition Temperature Measurements.** Unless otherwise stated, protein solutions were prepared on ice containing 30 $\mu$M H-$Z_R$-ELP, 0.05 $Z_E/Z_R$ ratio, and 0.5 M NaCl buffered with 10 mM $Na_2HPO_4$ for solutions at pH 6.0 or greater or 10 mM sodium succinate for solutions with pH lower than 6.0. Transition temperature was measured using an Applied Photophysics Chirascan-plus CD UV−Vis spectrophotometer. The temperature of each solution was increased from 5 to 60 °C at a ramp rate of 1 °C/min in a 1 mL quartz cuvette. The optical density (OD) of the solution at 400 nm was measured every minute, and the transition temperature was taken as the last point where the slope switched from being positive to negative (inflection point), as described in our previous work.[32,33]

**pH Transition Measurements.** Protein solutions were mixed on ice at each designated pH. They were then incubated in a BioTek Instrument Synergy H4 at 30, 37, or 42 °C as the OD at 400 nm of the solution was measured for 1 h in triplicate. The reported values represent the average of the maximum OD 400. The pH transition was taken as the halfway point between the OD 400 at the maximum and minimum turbidities.

**Dynamic Light Scattering.** To determine the size of structures that formed, DLS (Malvern Instruments Zetasizer NanoZS) was performed using intensity mode with a 4 mW He−Ne laser with a wavelength of 633 nm to detect backscattering (173°). The *Z*-average was used to report the size of vesicles.

**Small Angle X-ray Scattering.** SAXS data were collected using a Rigaku BioSAXS 2000 instrument operated by the Center for Structural Molecular Biology at the Oak Ridge National Laboratory. The wavelength, $\lambda$, was 1.542 Å, and the instrument was configured to measure momentum transfers $0.008 < Q < 0.70$ Å$^{-1}$, where $Q = (4\pi/\lambda)\sin(\theta)$ and $2\theta$ is the scattering angle. The sample temperature was maintained using a water bath connected to the automatic sample changer and sample position. Data acquisition and reduction used the SAXSLab 4.0.2 software provided with the instrument by Rigaku. All data were corrected for the solvent background scattering. Data analysis was performed with SasView (https://www.sasview.org) and used a superposition of the lamellar form factor (LFF) and the monodisperse Gaussian coil (MGC) model. Data were fit over a *Q*-range of $0.008 < Q < 0.35$ Å$^{-1}$.

## RESULTS AND DISCUSSION

**Characterizing the Effects of pH on Vesicle Self-Assembly.** In order to determine the pH responsiveness of the H-$Z_R$-ELP variants, the transition temperature of ELP as a function of solution pH was measured in solutions containing 30 $\mu$M H-$Z_R$-ELP, 1.5 $\mu$M mCherry-$Z_E$, 0.5 M NaCl, and 10 mM sodium phosphate (dibasic, for pH ≥ 6.0) or 10 mM sodium succinate (pH 5.5) to maintain a stable pH buffer (Figure 2a). This mCherry-$Z_E$ concentration and salt concentration were chosen because we have done extensive characterization of the system under similar conditions in the past work.[29,31−34] Because mCherry-$Z_E$ is a critical component to the vesicles, it was included in the solution during the transition temperature measurements to give a more accurate measurement of the transition temperature during vesicle self-assembly, as the ELP transition temperature is affected by the concentration of co-solutes.[15] Although the $T_t$ of ELPs is affected by the salt type, switching between the 10 mM sodium succinate and the 10 mM sodium phosphate buffers likely has a negligible effect on the $T_t$ because the sodium chloride concentration is 50 times that of the minority salt component.[28,38]

The transition temperature of mixtures of mCherry-$Z_E$ and each H-$Z_R$-ELP variant was found by measuring the OD of the solution at 400 nm as a function of temperature and is represented by the inflection point in the turbidity versus temperature profile (Figure 2b−d). The $T_t$ of $H_{15}$-$Z_R$-ELP could not be determined at pH 7.5 or 8.0 due to the hydrophobicity of histidine at elevated pH because it was lower than the lowest achievable temperature of the instrument (5 °C).[26] However, in general, this data demonstrated that each of the H-$Z_R$-ELP variants was pH-sensitive because as the pH of the solution was reduced, the $T_t$ of H-$Z_R$-ELP variants rose considerably. An


https://doi.org/10.1021/acs.biomac.2c00562
Biomacromolecules XXXX, XXX, XXX−XXX

increase in the transition temperature implies that the ELP is becoming more hydrophilic as the pH of the solution is reduced.

Additionally, the turbidity profiles indicated that vesicles formed above pH 6.5 for all three variants. Vesicle formation was confirmed when the turbidity profile plateaus after reaching its maximum value because hollow vesicles stay suspended in solution as stable colloids.[31] If the protein does not transition into vesicles, the dense protein coacervates settled to the bottom of the cuvette causing the turbidity to decrease after reaching a maximum, as in Figure 2c at pH 5.5 and Figure 2d at pH 6.0.

This data also demonstrated that increasing the number of histidines in the guest position of the ELP leads to an enhanced pH response. The change in $T_t$ of $H_5$-$Z_R$-ELP upon increasing pH from 5.5 to 8.0 is 9 °C compared to 14 °C for $H_{10}$-$Z_R$-ELP. $H_{15}$-$Z_R$-ELP exhibits a more drastic response to changes in pH, though the exact change is unknown due to its reduced, immeasurable $T_t$ at pH 8.0. Adding additional histidines also increases the pH responsiveness of the ELP. When the pH is increased from 5.5 to only 7.0, the change in transition temperature is 16 °C. This trend is consistent with the hydrophobicity scale of amino acids based on the ELP inverse transition temperature.[26] According to this hydrophobicity scale, histidine at pH 8.0 is the fourth most hydrophobic amino acid, while the hydrophobicity of histidine at pH 4.0 is comparable to the hydrophilic amino acids lysine and glutamate. Therefore, at pH 8.0, increasing the number of histidines in the guest residue leads to a significantly more hydrophobic ELP, and a considerable reduction in the transition temperature of the ELP compared to the ELPs with less histidines in the guest residue. Because at low pH histidine is a hydrophilic amino acid, incorporating more histidine residues leads to elevated transition temperature of ELP. Since the vesicles exhibit different degrees of pH sensitivity, they exhibit different optimal operating temperatures. For example, from the turbidity profiles, we determined that at 42 °C, $H_5$-$Z_R$-ELP will form stable vesicles even at pH 5.5 and therefore would not disassemble upon reduction of pH. Conversely, $H_{15}$-$Z_R$-ELP vesicles would likely disassemble at 42 °C below pH 6.5.

Next, in order to determine the pH transition ($pH_t$) of the ELP variants, 4 °C mixtures of mCherry-$Z_E$ and H-$Z_R$-ELP at pH 4.0−8.0 were incubated at 37 °C for 1 h, while the turbidity was recorded. The maximum turbidity (OD at 400 nm) of each solution represents the degree to which ELP has transitioned from soluble to coacervates or vesicles. The maximum of turbidity versus time profiles was plotted as a function of pH to determine the $pH_t$ of the H-$Z_R$-ELP variants (Figure 3). The $pH_t$ region for all three H-$Z_R$-ELP variants is between pH 5.0 and 7.0,

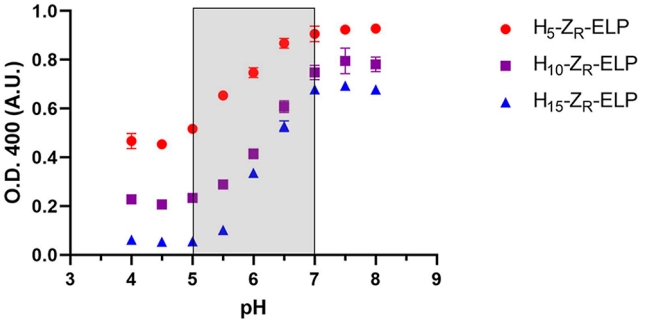


**Figure 3.** pH Transition of each variant as a function of pH at 37 °C. The gray region denotes the region where the pH transition is occurring.

which corresponds to the pH range where histidine transitions from a neutral amino acid to a positively charged amino acid. The ELP response to reductions in pH was also much stronger with higher histidine content as there was a larger change in OD across the $pH_t$ region. The OD measurements also show that $H_{15}$-$Z_R$-ELP did not transition substantially when the pH is below 5.5 at 37 °C.

In order to observe pH-dependent vesicle assembly, three different operating temperatures were chosen based on the $T_t$ of the ELP. The operating temperatures that were chosen would result in the maximum turbidity being reached at pH 8.0−7.0 but then decrease for pH 6.5 and below based on the turbidity profiles from Figure 2. Because $H_5$-$Z_R$-ELP had the least number of histidines, it exhibited pH transition behavior at a lower temperature, 30 °C. $H_{10}$-$Z_R$-ELP and $H_{15}$-$Z_R$-ELP required higher operating temperatures of 37 and 42 °C, respectively. To demonstrate that vesicle self-assembly was pH-responsive at these different operating temperatures, mCherry-$Z_E$ and H-$Z_R$-ELP variants were mixed at 4 °C and pH values between 5.5 and 8.0. The mixture was then taken off ice and immediately incubated at 30, 37, and 42 °C, while the turbidity was recorded over a 1-hour period (Figure 4a−c). In the first 10 min, the turbidity increases sharply for samples at high pH and slowly for samples at lower pH. Below pH 7.0, the maximum turbidity of the mixtures decreased and the time to reach the maximum increased, indicating that the vesicle self-assembly is affected by pH. For $H_{10}$-$Z_R$-ELP and $H_{15}$-$Z_R$-ELP, the turbidity profiles at pH 6.5 and 6.0 decrease over time after reaching the maximum, indicating the formation of unstable structures, not vesicles. At pH 5.5, the self-assembly is severely disrupted as the maximum turbidity does not reach even half of the turbidity of the mixtures at pH 7.0. This indicates that a much smaller fraction of the ELP is undergoing a hydrophobic transition.

The hydrodynamic diameters of the structures were measured by DLS (Figures 4d, S2−S4 and Tables S1−S3). DLS showed that the average diameter of vesicles increases as pH of the solution decreases for all three variants. However, quality DLS data could not be obtained at low pH due to an increase in the polydispersity of the vesicles or the formation of unstable coacervates for $H_{10}$-$Z_R$-ELP and $H_{15}$-$Z_R$-ELP. These results were corroborated by epifluorescence microscopy, which consistently showed that the vesicles formed under acidic conditions were larger than the vesicles formed under alkaline conditions when the histidine is deprotonated (Figure 4e). Although the turbidity profiles indicated stable vesicle formation and quality DLS results were obtained for $H_5$-$Z_R$-ELP at pH 5.5, microscopy revealed that coacervates remained the most prevalent structures at 30 °C (Figure S5).

Together, these results demonstrate that (1) incorporating histidine into the guest residue of ELP imparts pH sensitivity into the vesicles, (2) the amount of histidine in the ELP affects the pH responsiveness of the vesicles, and (3) when vesicles are formed from H-$Z_R$-ELP at lower pH, they tend to be larger. All three of these phenomena can be explained by the properties of ELP, which change with guest residue hydrophilicity and charge. Histidine is widely considered a more hydrophilic amino acid compared to valine at neutral pH.[39−41] Substituting valine with histidine leads to an increase in the ELP transition temperature and the hydrophilicity of the ELP in general. Additionally, as the pH of the solution is reduced, higher fractions of histidine become protonated causing intra- and intermolecular electrostatic repulsion between the charged groups, thereby increasing ELP solubility in water. Both effects serve to disrupt the


https://doi.org/10.1021/acs.biomac.2c00562
Biomacromolecules XXXX, XXX, XXX−XXX

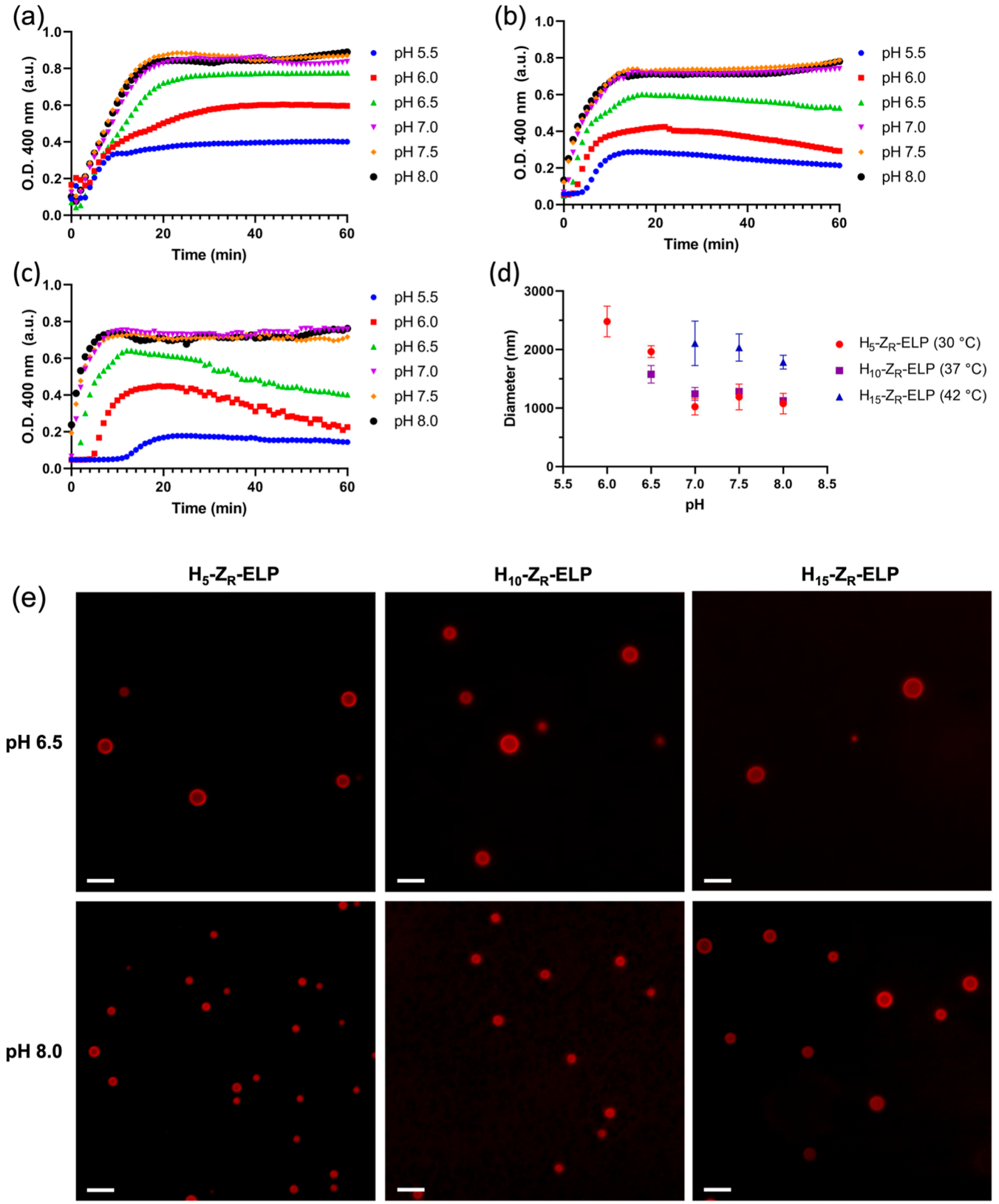


**Figure 4.** pH-responsive behavior for $H_5$-$Z_R$-ELP, $H_{10}$-ZR-ELP, and $H_{15}$-ZR-ELP vesicles. Turbidity profiles of each H-$Z_R$-ELP variant at different pH values for the chosen operating temperatures: (a) $H_5$-$Z_R$-ELP at 30 °C, (b) $H_{10}$-$Z_R$-ELP at 37 °C, and (c) $H_{15}$-$Z_R$-ELP at 42 °C. (d) Average hydrodynamic diameter and (e) epifluorescence microscopy images of $H_5$-$Z_R$-ELP (30 °C), $H_{10}$-$Z_R$-ELP (37 °C), and $H_{15}$-$Z_R$-ELP (42 °C) vesicles. Scale bars are 2 $\mu$m.


https://doi.org/10.1021/acs.biomac.2c00562
*Biomacromolecules* XXXX, XXX, XXX−XXX

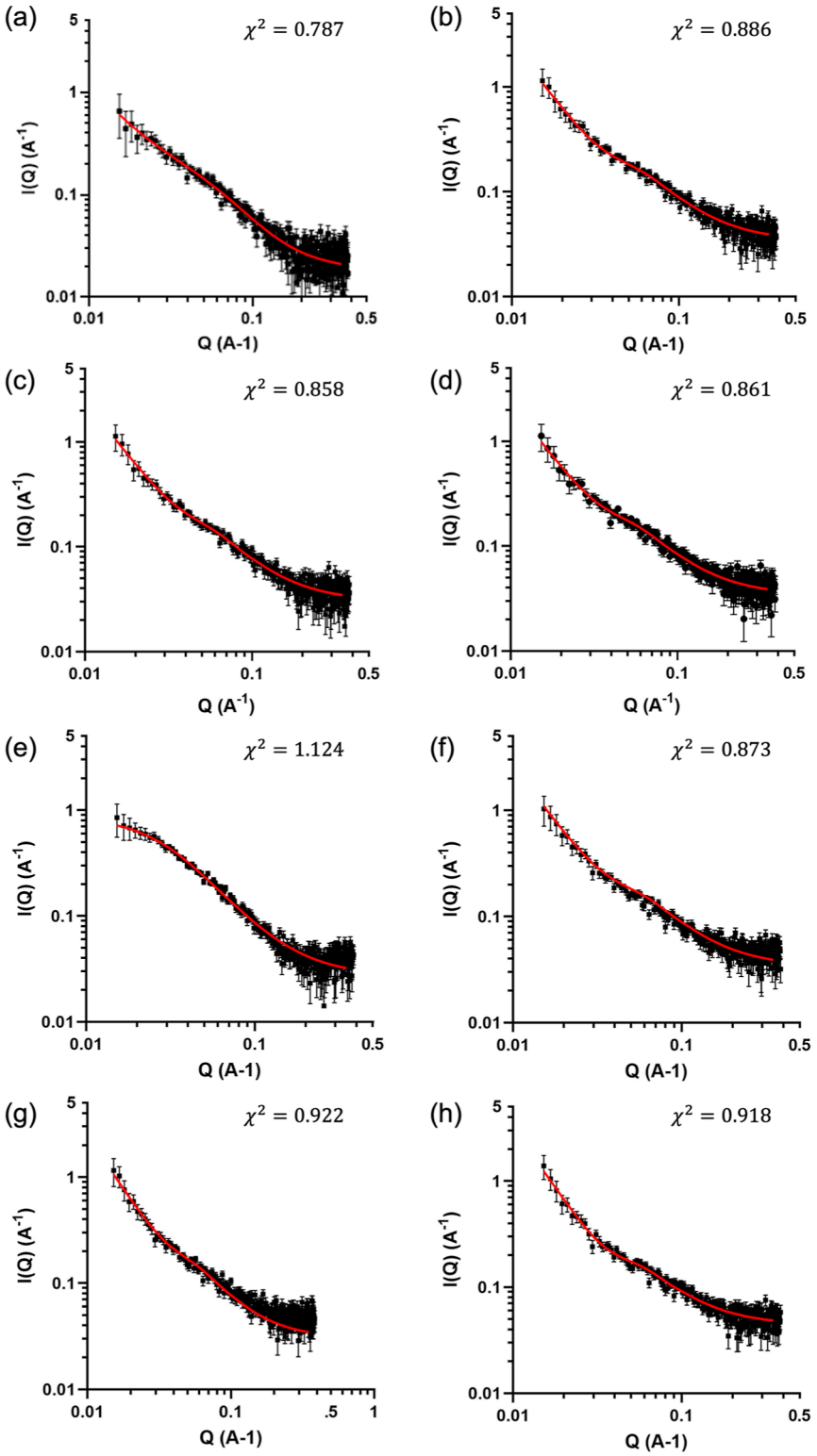


**Figure 5.** SAXS data for $H_5$-$Z_R$-ELP and $H_{15}$-$Z_R$-ELP for vesicles formed at different pH values: $H_5$-$Z_R$-ELP at (a) pH 5.50, (b) pH 6.75, (c) pH 7.00, and (d) pH 8.00; $H_{15}$-$Z_R$-ELP at (e) pH 5.50, (f) pH 6.75, (g) pH 7.00, and (h) pH 8.00. Black squares represent experimental data, and red lines are the fit using Lamellar and Gaussian coil models. Reduced chi squared values for each fit are shown in the top right of each fit.

compact, hydrophobic structure that usually forms when ELP is heated, forcing ELP to adopt a more extended, hydrophilic conformation according to circular dichroism (Figure S6).

**Investigating the Effects of pH on the ELP Structure with Small Angle X-ray Scattering.** There are two potential reasons why reducing the pH would increase the size of protein vesicles. First, the increased hydrophilicity of the ELP leads to partial unfolding of the compact structure compared to higher pH, increasing membrane thickness and the overall volume of the hydrophobic block.[42−44] This behavior has been observed in polymersomes when the hydrophobic block becomes hydrophilic due to protonation.[45] Another potential reason for larger


https://doi.org/10.1021/acs.biomac.2c00562
Biomacromolecules XXXX, XXX, XXX−XXX

**Table 2. Summary of SAXS Data Analysis and Fitting Parameters**[a]

| | $H_5$-$Z_R$-ELP | | | | $H_{15}$-$Z_R$-ELP | | | |
|---|---|---|---|---|---|---|---|---|
| pH | thickness (nm) | $R_g$ (nm) | LFF scale | MGC scale | thickness (nm) | $R_g$ (nm) | LFF scale | MGC scale |
| 5.50 | 2.64 ± 0.46 | 2.91 ± 0.32 | 0.53 ± 0.13 | 0.17 ± 0.03 | N/A | 5.24 ± 0.19 | N/A | 0.84 ± 0.46 |
| 6.75 | 13.15 ± 1.02 | 3.01 ± 0.16 | 0.28 ± 0.03 | 0.28 ± 0.02 | 13.12 ± 1.46 | 3.53 ± 0.29 | 0.25 ± 0.04 | 0.29 ± 0.03 |
| 7.00 | 13.32 ± 1.45 | 3.43 ± 0.22 | 0.26 ± 0.03 | 0.30 ± 0.03 | 12.64 ± 1.29 | 3.28 ± 0.25 | 0.28 ± 0.04 | 0.25 ± 0.03 |
| 8.00 | 13.83 ± 1.31 | 2.85 ± 0.21 | 0.24 ± 0.03 | 0.29 ± 0.02 | 13.81 ± 1.10 | 3.24 ± 0.17 | 0.24 ± 0.03 | 0.25 ± 0.02 |

[a]The parameter "thickness" is the membrane thickness in the LFF model, while "LFF Scale" refers to the multiplicative constant applied to the LFF that was determined during data fitting. Similarly, $R_g$ is the radius of gyration parameter of the MGC model and "MGC scale" is the multiplicative constant determined during data fitting. When the data did not indicate the presence of the lamellar structure, the LFF was not used during data fitting, and the membrane thickness and LFF scale are not reported (denoted N/A).

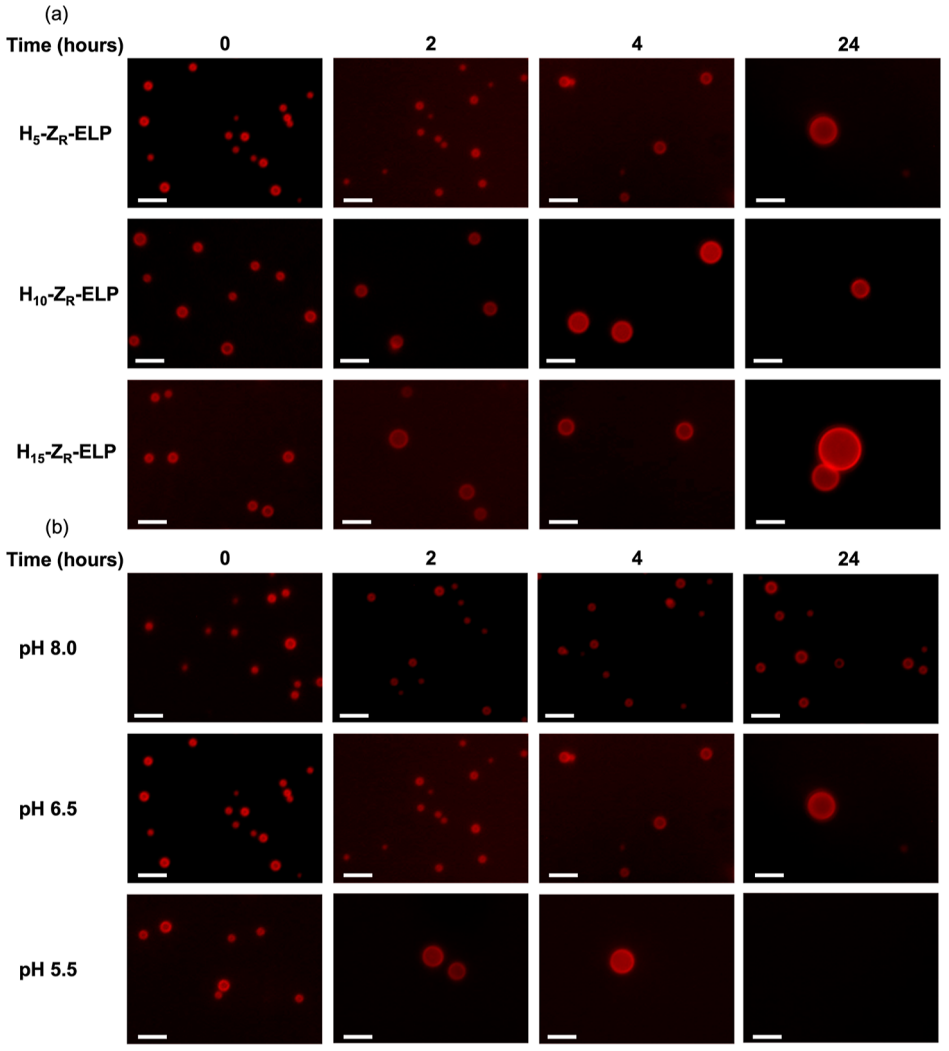


**Figure 6.** Epifluorescence microscopy demonstrates the disassembly of vesicles at low pH. (a) Vesicles were assembled at pH 8.0 from mCherry-$Z_E$ and each H-ZR-ELP variant. The pH was reduced to pH 6.5, and images were taken at 0, 2, 4, and 24 h (b) mCherry-$Z_E$/$H_5$-ZR-ELP vesicles were formed at pH 8.0, and then, the pH was reduced to 6.5 and 5.5 and vesicle growth and disassembly were observed over time. Scale bars are 2 $\mu$m.

vesicles at more acidic pH is the amount of time the vesicles spend in their transition state prior to maximum OD. In past studies, we have shown that the time vesicles spend in the coacervate transition stage impacts vesicle size.[33] When the coacervate stage lasts longer, the coacervates merge and grow, which leads to the formation of larger vesicles at the completion of the transition. Above pH 7.0, the turbidity profiles look similar for all three H-$Z_R$-ELP variants. However, below pH 7.0, the turbidity increases more slowly, leading to longer transition times, which could increase the vesicle size (Figure 4a–c). In order to understand why the protein vesicles were larger at high pH, we sought to measure the membrane thickness of the $H_5$-$Z_R$-ELP and $H_{15}$-$Z_R$-ELP protein vesicles formed at different pH values using SAXS.

The average hydrodynamic diameters of the vesicles in these experiments were close to or greater than 1 $\mu$m. Since the membrane thickness of the vesicles was estimated to be on the order of 10 nm based on our previous work,[34] the vesicles could be seen as infinite lamellar sheets, and therefore, a LFF was chosen to model this system.[46] The Debye Gaussian coil model


https://doi.org/10.1021/acs.biomac.2c00562
Biomacromolecules XXXX, XXX, XXX−XXX

for polymers, which can also be used to model unfolded proteins, was used to obtain the radius of gyration for the soluble proteins that remained in solution.[47] Accordingly, the SAXS data were fit using a superposition of LFF and monodisperse Debye Gaussian coil models (MGC) (Figure 5). The thickness of vesicle membranes was approximately 13 nm, which was consistent with the thickness of single-layered vesicles in our previous studies.[34] The SAXS results demonstrated that the pH of the solution does not impact the overall membrane thickness significantly over the pH range tested when vesicles are present (Table 2). This indicates that the ELP is likely not partially unfolded by moderate pH changes and only unfolded when the pH of the solution was decreased to pH 5.5 for $H_{15}$-$Z_R$-ELP. More evidence of this is seen at pH 5.5, where $H_5$-$Z_R$-ELP forms predominately coacervates, and $H_{15}$-$Z_R$-ELP is largely soluble. The radius of gyration ($R_g$) of the soluble portion was approximately the same across all pH values for $H_5$-$Z_R$-ELP/mCherry-$Z_E$ mixtures, even at pH 5.5 when coacervates are present. The negligible changes in $R_g$ indicated that $H_5$-$Z_R$-ELP remained largely in its compact state at pH 5.5, even though the protein gained charge and became more hydrophilic. The increased hydrophilicity prevents the ELP from forming highly ordered structures, such as vesicles, but there is sufficient hydrophobic character for the formation of lesser ordered coacervate structures. Meanwhile, $R_g$ increased from approximately 3 to 5 nm for mixtures of $H_{15}$-$Z_R$-ELP/mCherry-$Z_E$ when the pH is reduced from 6.75 to 5.5, as the ELP switches from vesicles to soluble protein. The large increase in $R_g$ at pH 5.5 is likely caused by complete unfolding of the ELP at low pH due to the substantial amount of positive charge on the 15 histidine residues. The protonated histidine increased the favorable interactions between water and the ELP, preventing association of the ELP into higher ordered aggregates.[30]

**Lowering pH Triggers Vesicle Disassembly.** In previous sections, the effects of pH were shown on the assembly of the vesicles formed at different pH values. Here, we discuss the effects of lowering the pH on vesicles assembled at pH 8.0. To observe the disassembly of vesicles, the vesicles were imaged at 2, 4, and 24 h after reducing the pH of the solution from 8.0 to 6.5 or 5.5. DLS was not performed on samples when the pH was reduced because polydispersity became too high to obtain quality DLS results. Two hours after reducing the pH of $H_{10}$ and $H_{15}$-$Z_R$-ELP from 8.0 to 6.5, noticeable differences in the number of vesicles and their relative sizes occurred (Figures 6 and S7). After 4 h and especially after 24 h, the vesicles appeared to be considerably larger and fewer in number. Ultimately, at pH 5.5, no vesicles were present after 24 h. Because there were fewer vesicles present and the vesicles that were present were typically substantially larger, we hypothesized that the increased hydrophilicity of the ELP must form local intermediate structures that promote vesicle fusion and the formation of larger vesicles that eventually disassemble. This behavior is seen in liposomes and lipid nanoparticles where the formation of hexagonal phases can be responsible for membrane fusion.[48] Additionally, polymersome fusion can be initiated by membrane deformation that results in membrane fusion and the formation of tubesomes.[49] The formation of larger vesicles could also be attributed to Ostwald ripening, which occurs when smaller particles dissolve, and then, the soluble components deposit onto larger particles.[50]

To determine whether membranes were fusing, we synthesized vesicles from mCherry-$Z_E$/$H_5$-$Z_R$-ELP and superfolder green fluorescent protein-$Z_E$ (sfGFP-$Z_E$)/$H_5$-$Z_R$-ELP at pH 7.5 (Figure 7a,b). One hour after vesicle formation, the red and green vesicles were mixed either at pH 7.5 or pH 6.5 (Figure 7b,c). Mixed mCherry-$Z_E$ and sfGFP-$Z_E$ vesicles at pH 7.5 retained their original structure and were mostly homogeneous red or green vesicles. However, when the mixed vesicle pH was reduced to pH 6.5, the formation of fused, heterogeneous, yellowish vesicles was observed. The vesicles were also irregularly shaped, likely due to differences in the size of the red and green vesicles or packing differences between mCherry-$Z_E$ and sfGFP-$Z_E$.

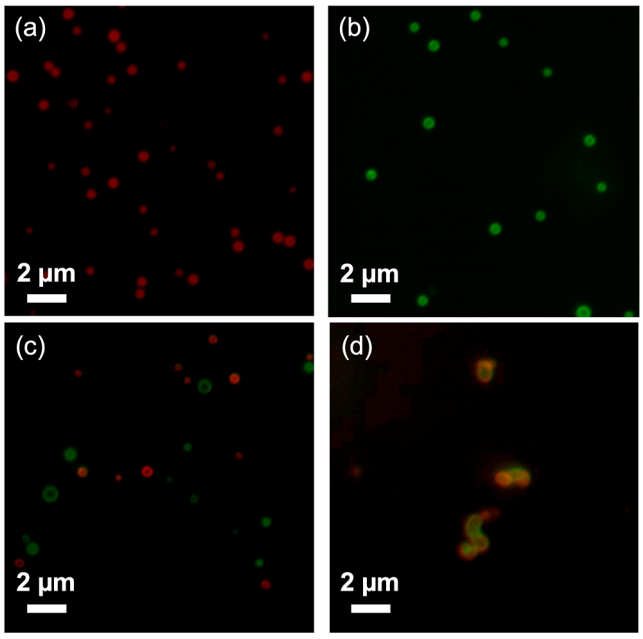


**Figure 7.** Epifluorescence microscopy demonstrating vesicle fusion upon reduction of pH 7.5 to pH 6.5. (a) mCherry-$Z_E$/$H_5$-$Z_R$-ELP vesicles at pH 7.5. (b) sfGFP-$Z_E$/$H_5$-$Z_R$-ELP vesicles at pH 7.5. (c) Mixture of mCherry-$Z_E$/$H_5$-$Z_R$-ELP and sfGFP-$Z_E$/$H_5$-$Z_R$-ELP vesicles at pH 7.5. (d) Heterogeneously fused mCherry-$Z_E$/$H_5$-$Z_R$-ELP and sfGFP-$Z_E$/$H_5$-$Z_R$-ELP vesicles made by reducing the mixed vesicle pH to 6.5 and waiting 1 h.

## CONCLUSIONS

In this work, the guest residue of ELP was modified to histidine to develop pH-sensitive vesicles composed entirely of fusion proteins. First, we investigated the ability of vesicles to form at different pH values and showed that the pH during formation affects the ELP transition, the structures that form (coacervate or vesicle), and the diameter of the vesicles that form. Next, we demonstrated that the mechanism for the changes in vesicle diameter as a function of pH is likely related to a change in the amount of time spent in the coacervate stage. This result was demonstrated by SAXS and showed that the $R_g$ of the protein and the membrane thickness remain unchanged when vesicles with assembled in lower pH solutions. Instead, $R_g$ only changed when the pH was reduced to pH 5.5 and then self-assembly of supramolecular structures was entirely disrupted. Lastly, we demonstrated pH-controlled disassembly of vesicles with epifluorescence microscopy. This work demonstrated the tunability of protein vesicles and the ability to develop them for stimuli responsiveness, expanding their potential in applications ranging from synthetic biology to microreactors or drug delivery. Though the vesicles used in this work were


https://doi.org/10.1021/acs.biomac.2c00562
Biomacromolecules XXXX, XXX, XXX−XXX

approximately 1 $\mu$m in diameter, we have previously developed methods to synthesize globular protein vesicles that are 100−200 nm in diameter, making them more suitable for drug-delivery applications.[29,32] In future work, we will incorporate pH sensitivity into smaller vesicles for use in drug-delivery applications.

## ■ ASSOCIATED CONTENT

### Supporting Information

The Supporting Information is available free of charge at https://pubs.acs.org/doi/10.1021/acs.biomac.2c00562.

Epifluorescence images of mCherry-$Z_E$/$H_5$-$Z_R$-ELP at pH 5.50 and 6.00, circular dichroism, SDS-PAGE gels of purified H-$Z_R$-ELPs, size distributions of vesicles as a function of pH, and TEM images of vesicles (PDF)

## ■ AUTHOR INFORMATION


### Corresponding Author

**Julie A. Champion** − *School of Chemical and Biomolecular Engineering, Georgia Institute of Technology, Atlanta, Georgia 30332, United States;* orcid.org/0000-0002-0260-9392; Email: julie.champion@chbe.gatech.edu

### Authors

**Dylan R. Dautel** − *School of Chemical and Biomolecular Engineering, Georgia Institute of Technology, Atlanta, Georgia 30332, United States*

**William T. Heller** − *Neutron Scattering, Oak Ridge National Laboratory, Oak Ridge, Tennessee 37831, United States;* orcid.org/0000-0001-6456-2975

Complete contact information is available at: https://pubs.acs.org/10.1021/acs.biomac.2c00562


### Notes

The authors declare no competing financial interest.

## ■ ACKNOWLEDGMENTS

This research was financially supported by the National Science Foundation Division of Materials Research, under award number 1709428, and M.T. Campagna. The authors gratefully acknowledge Profs. D.A. Tirrell and K. Zhang for AF-IQ *E. coli*and $Z_R$-ELP plasmid, Dr. Wellington Leite for training and assistance with SAXS, and Jamellah Jackson for her assistance with characterization. This work was performed in part at the Georgia Tech Institute for Electronics and Nanotechnology, a member of the National Nanotechnology Coordinated Infrastructure, which is supported by the National Science Foundation (grant no. ECCS-2025462). We wish to acknowledge the core facilities at the Parker H. Petit Institute for Bioengineering and Bioscience at the Georgia Institute of Technology for the use of their shared equipment, services, and expertise. Funding for the CSMB, which supports the SAXS instrument used, is provided by the Office of Biological & Environmental Research in the Department of Energy's Office of Science. A portion of this research used resources at the High Flux Isotope Reactor and the Spallation Neutron Source, a DOE Office of Science User Facility operated by the Oak Ridge National Laboratory.

## ■ REFERENCES


(1) van Dongen, S. F. M.; Nallani, M.; Cornelissen, J. J. L. M.; Nolte, R. J. M.; van Hest, J. C. M. A Three-Enzyme Cascade Reaction through Positional Assembly of Enzymes in a Polymersome Nanoreactor. *Chem.—Eur. J.* **2009**, *15*, 1107−1114.

(2) Gaitzsch, J.; Huang, X.; Voit, B. Engineering Functional Polymer Capsules toward Smart Nanoreactors. *Chem. Rev.* **2016**, *116*, 1053−1093.

(3) Dicheva, B. M.; ten Hagen, T. L. M.; Schipper, D.; Seynhaeve, A. L. B.; van Rhoon, G. C.; Eggermont, A. M. M.; Koning, G. A. Targeted and Heat-Triggered Doxorubicin Delivery to Tumors by Dual Targeted Cationic Thermosensitive Liposomes. *J. Controlled Release* **2014**, *195*, 37−48.

(4) Hindley, J. W.; Elani, Y.; McGilvery, C. M.; Ali, S.; Bevan, C. L.; Law, R. v.; Ces, O. Light-Triggered Enzymatic Reactions in Nested Vesicle Reactors. *Nat. Commun.* **2018**, *9*, 1093.

(5) Lamichhane, N.; Udayakumar, T. S.; D'Souza, W. D.; Simone II, C. B.; Raghavan, S. R.; Polf, J.; Mahmood, J. Liposomes: Clinical Applications and Potential for Image-Guided Drug Delivery. *Molecules* **2018**, *23*, 288.

(6) Rideau, E.; Dimova, R.; Schwille, P.; Wurm, F. R.; Landfester, K. Liposomes and Polymersomes: A Comparative Review towards Cell Mimicking. *Chem. Soc. Rev.* **2018**, *47*, 8572−8610.

(7) Hu, X.; Zhang, Y.; Xie, Z.; Jing, X.; Bellotti, A.; Gu, Z. Stimuli-Responsive Polymersomes for Biomedical Applications. *Biomacromolecules* **2017**, *18*, 649−673.

(8) Che, H.; van Hest, J. C. M. Stimuli-Responsive Polymersomes and Nanoreactors. *J. Mater. Chem. B* **2016**, *4*, 4632−4647.

(9) Onaca, O.; Enea, R.; Hughes, D. W.; Meier, W. Stimuli-Responsive Polymersomes as Nanocarriers for Drug and Gene Delivery. *Macromol. Biosci.* **2009**, *9*, 129−139.

(10) Felber, A. E.; Dufresne, M. H.; Leroux, J. C. PH-Sensitive Vesicles, Polymeric Micelles, and Nanospheres Prepared with Polycarboxylates. *Adv. Drug Delivery Rev.* **2012**, *64*, 979−992.

(11) Yang, H.; Wang, Q.; Li, Z.; Li, F.; Wu, D.; Fan, M.; Zheng, A.; Huang, B.; Gan, L.; Zhao, Y.; Yang, X. Hydrophobicity-Adaptive Nanogels for Programmed Anticancer Drug Delivery. *Nano Lett.* **2018**, *18*, 7909−7918.

(12) Callahan, D. J.; Liu, W.; Li, X.; Dreher, M. R.; Hassouneh, W.; Kim, M.; Marszalek, P.; Chilkoti, A. Triple Stimulus-Responsive Polypeptide Nanoparticles That Enhance Intratumoral Spatial Distribution. *Nano Lett.* **2012**, *12*, 2165−2170.

(13) Simon, J. R.; Carroll, N. J.; Rubinstein, M.; Chilkoti, A.; López, G. P. Programming Molecular Self-Assembly of Intrinsically Disordered Proteins Containing Sequences of Low Complexity. *Nat. Chem.* **2017**, *9*, 509−515.

(14) Dreher, M. R.; Simnick, A. J.; Fischer, K.; Smith, R. J.; Patel, A.; Schmidt, M.; Chilkoti, A. Temperature Triggered Self-Assembly of Polypeptides into Multivalent Spherical Micelles. *J. Am. Chem. Soc.* **2008**, *130*, 687−694.

(15) MacEwan, S. R.; Chilkoti, A. Elastin-like Polypeptides: Biomedical Applications of Tunable Biopolymers. *Biopolymers* **2010**, *94*, 60−77.

(16) Ghosh, K.; Balog, E. R. M.; Sista, P.; Williams, D. J.; Kelly, D.; Martinez, J. S.; Rocha, R. C. Temperature-Dependent Morphology of Hybrid Nanoflowers from Elastin-like Polypeptides. *APL Mater.* **2014**, *2*, 021101.

(17) Qin, J.; Luo, T.; Kiick, K. L. Self-Assembly of Stable Nanoscale Platelets from Designed Elastin-like Peptide-Collagen-like Peptide Bioconjugates. *Biomacromolecules* **2019**, *20*, 1514−1521.

(18) Qin, J.; Sloppy, J. D.; Kiick, K. L. Fine Structural Tuning of the Assembly of ECM Peptide Conjugates via Slight Sequence Modifications. *Sci. Adv.* **2020**, *6*, 1−11.

(19) Luo, T.; David, M. A.; Dunshee, L. C.; Scott, R. A.; Urello, M. A.; Price, C.; Kiick, K. L. Thermoresponsive Elastin-b-Collagen-Like Peptide Bioconjugate Nanovesicles for Targeted Drug Delivery to Collagen-Containing Matrices. *Biomacromolecules* **2017**, *18*, 2539−2551.

(20) Ibrahimova, V.; Zhao, H.; Ibarboure, E.; Garanger, E.; Lecommandoux, S. Thermosensitive Vesicles from Chemically Encoded Lipid-Grafted Elastin-like Polypeptides. *Angew. Chem., Int. Ed.* **2021**, *60*, 15036−15040.

(21) Cox, B. A.; Starcher, B. C.; Urry, D. W. Coacervation of Tropoelastin Results in Fiber Formation. *J. Biol. Chem.* **1974**, *249*, 997−998.
(22) Reichheld, S. E.; Muiznieks, L. D.; Keeley, F. W.; Sharpe, S. Direct Observation of Structure and Dynamics during Phase Separation of an Elastomeric Protein. *Proc. Natl. Acad. Sci. U.S.A.* **2017**, *114*, E4408−E4415.
(23) Rauscher, S.; Pomès, R. The Liquid Structure of Elastin. *Elife* **2017**, *6*, No. e26526.
(24) Reguera, J.; Urry, D. W.; Parker, T. M.; McPherson, D. T.; Rodríguez-Cabello, J. C. Effect of NaCl on the Exothermic and Endothermic Components of the Inverse Temperature Transition of a Model Elastin-like Polymer. *Biomacromolecules* **2007**, *8*, 354−358.
(25) Urry, D. W.; Long, M. M.; Cox, B. A.; Ohnishi, T.; Mitchell, L. W.; Jacobs, M. The Synthetic Polypentapeptide of Elastin Coacervates and Forms Filamentous Aggregates. *Biochim. Biophys. Acta Protein Struct.* **1974**, *371*, 597−602.
(26) Urry, D. W.; Gowda, D. C.; Parker, T. M.; Luan, C.-H.; Reid, M. C.; Harris, C. M.; Pattanaik, A.; Harris, R. D. Hydrophobicity Scale for Proteins Based on Inverse Temperature Transitions. *Biopolymers* **1992**, *32*, 1243−1250.
(27) Meyer, D. E.; Chilkoti, A. Quantification of the Effects of Chain Length and Concentration on the Thermal Behavior of Elastin-like Polypeptides. *Biomacromolecules* **2004**, *5*, 846−851.
(28) Cho, Y.; Zhang, Y.; Christensen, T.; Sagle, L. B.; Chilkoti, A.; Cremer, P. S. Effects of Hofmeister Anions on the Phase Transition Temperature of Elastin-like Polypeptides. *J. Phys. Chem. B* **2008**, *112*, 13765−13771.
(29) Li, Y.; Champion, J. A. Photocrosslinked, Tunable Protein Vesicles for Drug Delivery Applications. *Adv. Healthcare Mater.* **2021**, *10*, 2001810.
(30) MacKay, J. A.; Callahan, D. J.; FitzGerald, K. N.; Chilkoti, A. Quantitative Model of the Phase Behavior of Recombinant PH-Responsive Elastin-like Polypeptides. *Biomacromolecules* **2010**, *11*, 2873−2879.
(31) Park, W. M.; Champion, J. A. Thermally Triggered Self-Assembly of Folded Proteins into Vesicles. *J. Am. Chem. Soc.* **2014**, *136*, 17906−17909.
(32) Dautel, D.; Champion, J. Protein Vesicles Self-Assembled from Functional Globular Proteins with Different Charge and Size. *Biomacromolecules* **2021**, *22*, 116−125.
(33) Jang, Y.; Hsieh, M. C.; Dautel, D.; Guo, S.; Grover, M. A.; Champion, J. A. Understanding the Coacervate-to-Vesicle Transition of Globular Fusion Proteins to Engineer Protein Vesicle Size and Membrane Heterogeneity. *Biomacromolecules* **2019**, *20*, 3494−3503.
(34) Jang, Y.; Choi, W. T.; Heller, W. T.; Ke, Z.; Wright, E. R.; Champion, J. A. Engineering Globular Protein Vesicles through Tunable Self-Assembly of Recombinant Fusion Proteins. *Small* **2017**, *13*, 1700399.
(35) Moll, J. R. Designed Heterodimerizing Leucine Zippers with a Ranger of PIs and Stabilities up to 10-15 M. *Protein Sci.* **2001**, *10*, 649−655.
(36) Tan, R.; Shin, J.; Heo, J.; Cole, B. D.; Hong, J.; Jang, Y. Tuning the Structural Integrity and Mechanical Properties of Globular Protein Vesicles by Blending Crosslinkable and NonCrosslinkable Building Blocks. *Biomacromolecules* **2020**, *21*, 4336−4344.
(37) Park, W. M.; Champion, J. A. Two-Step Protein Self-Assembly in the Extracellular Matrix. *Angew. Chem., Int. Ed.* **2013**, *52*, 8098−8101.
(38) Kherb, J.; Flores, S. C.; Cremer, P. S. Role of Carboxylate Side Chains in the Cation Hofmeister Series. *J. Phys. Chem. B* **2012**, *116*, 7389−7397.
(39) Kyte, J.; Doolittle, R. F. A Simple Method for Displaying the Hydropathic Character of a Protein. *J. Mol. Biol.* **1982**, *157*, 105−132.
(40) Engelman, D. M.; Steitz, T. A.; Goldman, A. Identifying Nonpolar Transbilayer Helices in Amino Acid Sequences of Membrane Proteins. *Annu. Rev. Biophys. Biophys. Chem.* **1986**, *15*, 321−353.
(41) Eisenberg, D.; Schwarz, E.; Komaromy, M.; Wall, R. Analysis of Membrane and Surface Protein Sequences with the Hydrophobic Moment Plot. *J. Mol. Biol.* **1984**, *179*, 125−142.
(42) Nagarajan, R. Molecular Packing Parameter and Surfactant Self-Assembly: The Neglected Role of the Surfactant Tail. *Langmuir* **2002**, *18*, 31−38.
(43) Tanford, C. Thermodynamics of Micelle Formation: Prediction of Micelle Size and Size Distribution. *Proc. Natl. Acad. Sci. U.S.A.* **1974**, *71*, 1811−1815.
(44) Tanford, C. Theory of Micelle Formation in Aqueous Solutions. *J. Phys. Chem.* **1974**, *78*, 2469−2479.
(45) Liu, X.; Yaszemski, M. J.; Lu, L. Expansile Crosslinked Polymersomes for PH Sensitive Delivery of Doxorubicin. *Biomater. Sci.* **2016**, *4*, 245−249.
(46) Ma, G.; Barlow, D. J.; Lawrence, M. J.; Heenan, R. K.; Timmins, P. Small-Angle Neutron-Scattering Studies of Nonionic Surfactant Vesicles. *J. Phys. Chem. B* **2000**, *104*, 9081−9085.
(47) Receveur-Brechot, V.; Durand, D. How Random Are Intrinsically Disordered Proteins? A Small Angle Scattering Perspective. *Curr. Protein Pept. Sci.* **2012**, *13*, 55−75.
(48) Morgan, C. G.; Yianni, Y. P.; Sandhu, S. S.; Mitchell, A. C. Liposome Fusion and Lipid Exchange on Ultraviolet Irradiation of Liposomes Containing a Photochromic Phospholipid. *Photochem. Photobiol.* **1995**, *62*, 24−29.
(49) Varlas, S.; Keogh, R.; Xie, Y.; Horswell, S. L.; Foster, J. C.; O'Reilly, R. K. Polymerization-Induced Polymersome Fusion. *J. Am. Chem. Soc.* **2019**, *141*, 20234−20248.
(50) Kahlweit, M. Ostwald Ripening of Precipitates. *Adv. Colloid Interface Sci.* **1975**, *5*, 1−35.


https://doi.org/10.1021/acs.biomac.2c00562
*Biomacromolecules* XXXX, XXX, XXX−XXX